095172

Effect of Faulting on Fluid Flow in Porous Sandstones: Petrophysical Properties[1]

Marco Antonellini and Atilla Aydin[2]

ABSTRACT

Fault zone permeability in outcrop is quantified by detailed geologic mapping and by measurements using a minipermeameter. Deformation bands, zones of deformation bands, and slip planes are structural elements associated with successive stages in the evolution of a fault zone in porous sandstones. Deformation bands have a porosity about one order of magnitude less than the surrounding host rock and, on average, a permeability three orders of magnitude less than the surrounding host rock. The intensity of cataclasis and the clay content control the amount of permeability reduction as measured perpendicular to a band. The wall rock in proximity to slip planes can have permeabilities more than seven orders of magnitude less than the pristine sandstone. Capillary pressure within deformation bands is estimated to be 10–100 times larger than that in the surrounding host rock. Thus, deformation bands and slip planes can substantially modify fluid flow properties of a reservoir and have potential sealing capabilities with respect to a nonwetting phase, as evident in outcrop exposure.

INTRODUCTION

Faulting in granular materials generally causes cataclasis and changes in porosity. These processes may affect the quality of otherwise excellent reservoir rocks and, in multiphase flow, can cause compartmentalization and fault sealing (Nelson, 1985; Hardmann and Booth, 1991). Compartmentalization of adjacent porous reservoirs caused by fault sealing has been recognized in the Gulf Coast (Smith, 1980), in the Niger Delta (Weber and Daukoru, 1975; Seeburger et al., 1991), in California, and in Central Sumatra (Harding and Tuminas, 1988). Clay smearing or fault zone granulation are the mechanisms commonly invoked to explain this phenomenon (Smith, 1966, 1980; Downey, 1984; Watts, 1987; Bouvier et al., 1989). Furthermore, diagenetic processes in a fault zone can affect the spatial distribution of porosity and permeability in its proximity (Bevan, 1985).

The paper that we present is part of a larger project concerned with the outcrop study of fault zones in porous sandstones and with the characterization of their micro- and macroproperties. The objective is to assess the impact of fault zones on fluid flow and sealing in porous sandstones. In this paper, we quantify the microstructural and petrophysical properties of fault zones in sandstones. In another paper (Antonellini and Aydin, in preparation), we pay special attention to the geometry of fault zones, lateral continuity, and three-dimensional structure. This latter aspect is relevant when sealing across a fault zone is provided not only by cataclasis and granulation, but also by the contact between two formations with very different capillary pressures (e.g., sandstone and shale). The field portion of this study was conducted at Arches National Park in southeastern Utah (Figure 1).

Faulting in porous sandstones evolves from a single deformation band to a zone of deformation bands and then into a slip plane (Aydin, 1977, 1978; Aydin and Johnson, 1978, 1983; Antonellini et al., in press). Deformation bands are also called shear bands, shear fractures, granulation seams, Lüder bands, tabular compaction zones, or band faults; all these terms may be found in the literature. Nelson (1985), in his book on naturally fractured reservoirs, referred to these structures as "gouge-filled fractures." A deformation band is a thin (0.5–2 mm thick) "fault-like" tabular structure (Figure 2a) usually with large lateral continuity (Zhao and Johnson, 1991). Deformation bands can accommodate small amounts of offset (a few mil-

©Copyright 1994. The American Association of Petroleum Geologists. All rights reserved.

[1]Manuscript received, July 6, 1993; revised manuscript received, November 1, 1993; final acceptance, November 19, 1993.

[2]Rock Fracture Project and Department of Geological and Environmental Sciences, Stanford University, Stanford, California 94305-2115.

This work has been sponsored by the Rock Fracture Project at Stanford University. Additional funding has been provided by a McGee Award from the Geology Department and by a Phillips Fellowship to M. Antonellini. We thank David Goggin at Chevron Petroleum Technology Company (La Habra, California) for making the minipermeameter available and Doug Okada for help in the lab. Special thanks to Brian Quinn at Bechtel for help with the video image analysis system and to Ken Cruikshank for assistance during the field work. Reviews by D. Pollard, M. C. Cacas, R. Nelson, and J. H. Doveton have greatly improved the manuscript.

14675

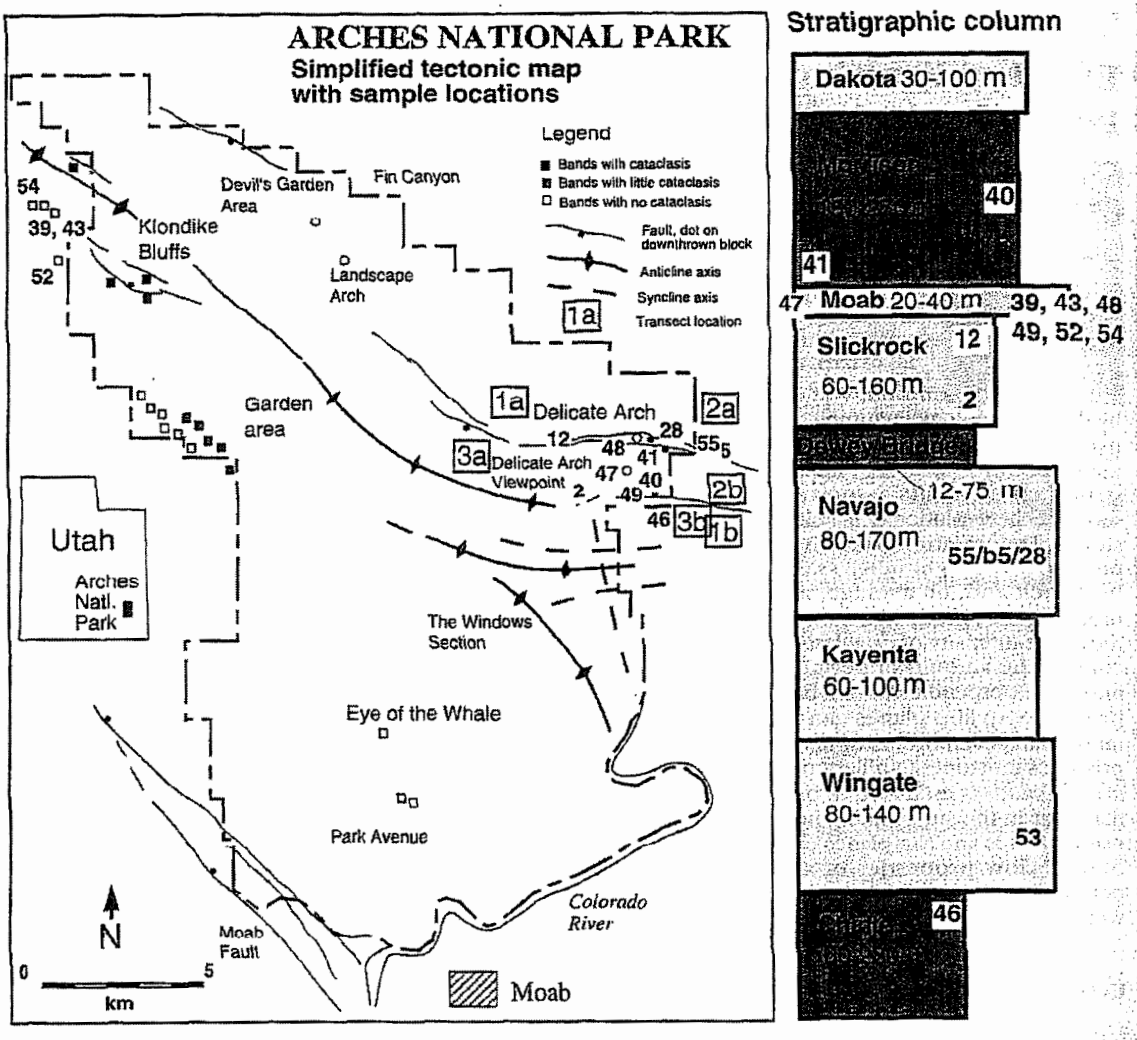

Figure 1—Simplified tectonic map of Arches National Park, Utah. Numbers indicate locations of selected samples for which permeability was determined. Numbers in the boxes represent transect locations. The stratigraphic column for the Arches National Park area is also represented; formation thicknesses are given in meters. Numbers in the column indicate the stratigraphic position of the sample.

limeters to a few centimeters) and are characterized by localized cataclasis and/or volume changes (Figure 2b). Many deformation bands may cluster in zones of deformation bands associated with offsets on the order of a few decimeters. Further offset (meters or tens of meters) is generally accommodated by the development of a slip plane, representing a displacement discontinuity in the rock body (Figure 3). Jamison and Stearns (1982) measured the spatial distribution of deformation bands near a fault zone with tens of meters offset in the Colorado National Monument and they found a clear correlation between high density of deformation bands and proximity to the fault. Engelder (1974) examined the relation between amount of slip and thickness of the gouge zone in a fault within the Precambrian sandstones of the Uinta Mountain Group (Utah); he found that the thickness of the gouge zone increased as the amount of slip was increased.

The petrophysical properties of deformation bands have been studied by Pittman (1981) in quartz sandstones of the Ordovician Simpson Group in

Oklahoma. He measured the three quantities necessary to characterize fluid behavior in a rock: porosity, permeability, and capillary pressure. Porosity measures the ability of a rock to store fluids. Permeability measures how easily a fluid can circulate through the pores of a rock. In practice, permeability represents a proportionality constant that links Darcy's law to rock properties. Capillary pressure, which is related to pore throat diameters, measures how well a water-saturated rock resists the invasion of a nonwetting second phase (hydrocarbons) driven by a gradient in pressure. Capillary pressure thus determines the sealing properties of a rock.

Pittman (1981) determined porosity and permeability from core plugs of fault zones. He noticed that both porosity and permeability decreased as the number of deformation bands increased. He measured porosity ranging from 2.8 to 29.6% and permeability ranging from 0.05 to 51.934 md (millidarcys).

Permeability and porosity measured in core plugs represent some form of an average of host rock and deformation band properties. In fact, deformation bands are so thin (a few millimeters) that a core plug 3/4 in (2 cm) in diameter, as used in conventional permeameters (Anderson, 1975), very likely would contain deformation band material, as well as host rock. The relative proportion of the two is difficult to measure. To avoid the problems related to averaging properties in a core plug, we used image analysis (Quinn, 1988; Full et al., 1984) and the minipermeameter (Goggin et al., 1988) to characterize the porosity and the permeability of material within a deformation band. Then, these data were used to quantify fault zone permeability at different scales. Mercury injection is not appropriate to measure capillary pressures within a single deformation band (1–2 mm in thickness), however, via image analysis, it is possible to characterize the pore network geometry and to evaluate its effect on sealing properties. The porosity and the permeability determined in the samples of deformation bands are functions of amount of cataclasis, clay content, and/or diagenetic precipitation of cement and authigenic minerals.

At Arches National Park in southeastern Utah (Figure 1), faulting developed in Mesozoic detrital rocks as a result of growth and subsequent collapse of a northwest-southeast-trending salt anticline (Doelling, 1985). Salt movement during growth of the anticline has been recorded as occurring from the Permian to Jurassic. Salt dissolution and collapse started later and probably are ongoing (Doelling, 1985). Deformation bands and fault zones formed in association with dif-

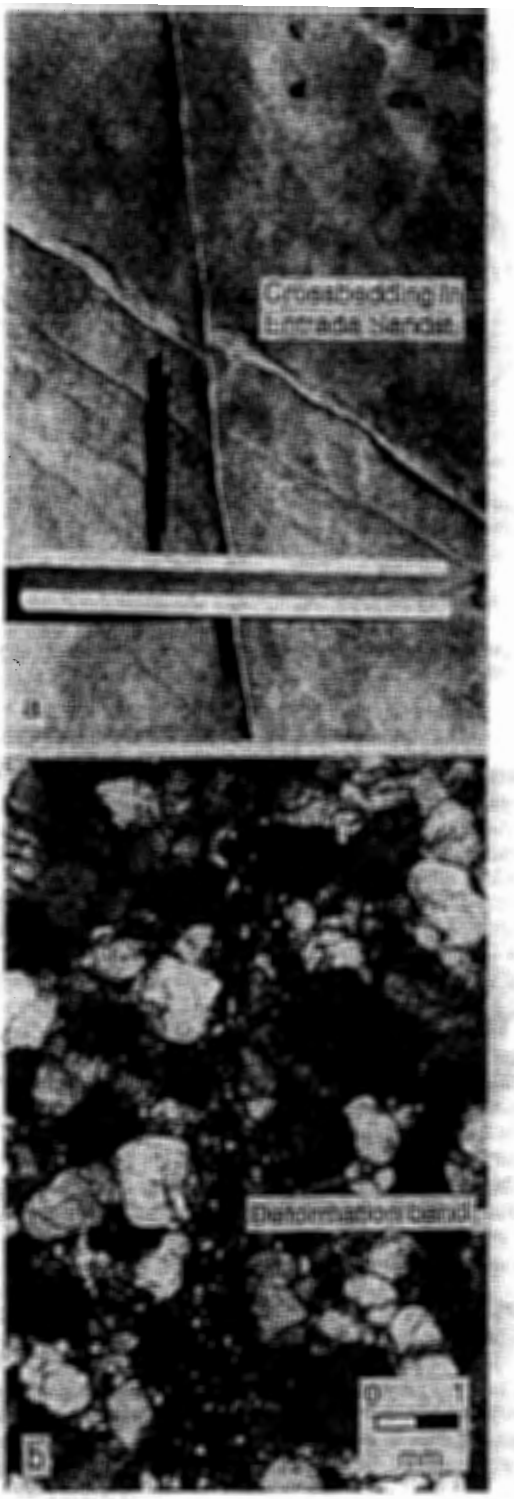

Figure 2—Photographs showing (a) deformation band in outcrop exposure and (b) thin section image of a deformation band (40×, cross nicols). Note the fine layer of cataclasite along the trace of the band.

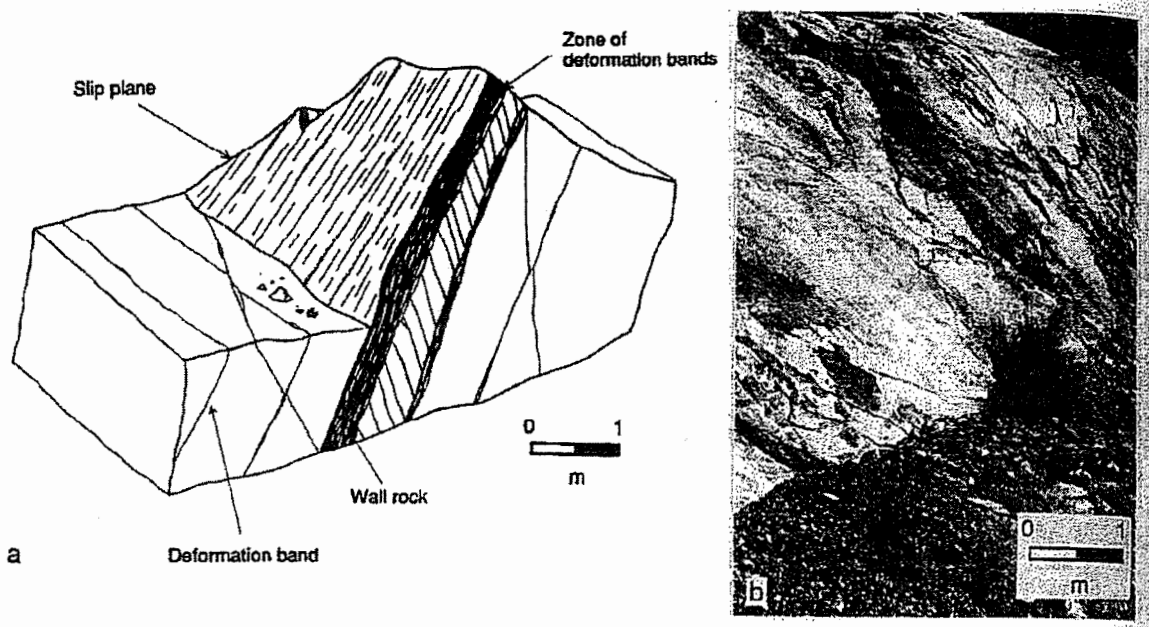

Figure 3—Slip plane in sandstone. (a) Schematic representation and terminology. (b) Photograph showing slip plane in Navajo Sandstone at Arches National Park.

ferent stages of salt anticline development (Antonellini et al., in press). Fault zones were mapped at different scales to document their geometry and, at the same time, samples from deformation bands and the wall rock of slip planes were collected for porosity and permeability determinations. Porosity was measured for specimens of different rock types, not restricted to those at Arches National Park. Permeability was measured on samples of the Triassic Chinle and the Jurassic Navajo, Entrada, and Morrison formations.

Evaluation of fluid flow through a localized low-permeability fault zone has to be performed at the scale appropriate for the problem under consideration and cannot be disconnected from the three-dimensional geometry and lateral continuity of the fault itself. This spatial aspect of fault permeability is critical for evaluating the sealing properties of a fault zone or set of faults and will be considered in another paper (Antonellini and Aydin, in preparation).

POROSITY OF DEFORMATION BANDS AND OF WALL ROCK ADJACENT TO SLIP PLANES

Video-image analysis and point counting of thin sections have been used to determine the two-dimensional porosity in deformation bands, in the boundary region of deformation bands, and in the host rock. Thin section images are transferred from a video camera to a PC-based image analysis system supported by an RTI (Recognition Technology, Inc.) vision engine. The images are segmented to separate pore space from mineral grains, and porosity is determined by automatic pixel counting (Full et al., 1984; Ehrlich et al., 1985; Antonellini et al., in press).

Porosity determinations are presented in Figure 4a for the host rocks and for the deformation bands in sandstones from Arches National Park (Utah), the St. Peter Sandstone in Kentland (northern Indiana), the Aztec Sandstone in the Valley of Fire (southern Nevada), and the Pismo Formation near Pismo Beach (central California). A detailed analysis of the relations between porosity in the host rock, porosity in the band, and the associated microstructure is given in another paper (Antonellini et al., in press). Where cataclasis is well developed in the bands, and where the porosity of the host rock is more than 15–20%, the porosity in the bands is about one order of magnitude less than that of the host rock. If the porosity of the host rock is relatively low, the drop in porosity of the band is less pronounced.

In the Moab member of the Entrada Sandstone, the porosity of the host rock is extremely variable (4–28%), as is the porosity of the bands (<1–18%; see Figure 4b, c). This variability is attributed to different microstructures that have been observed in thin

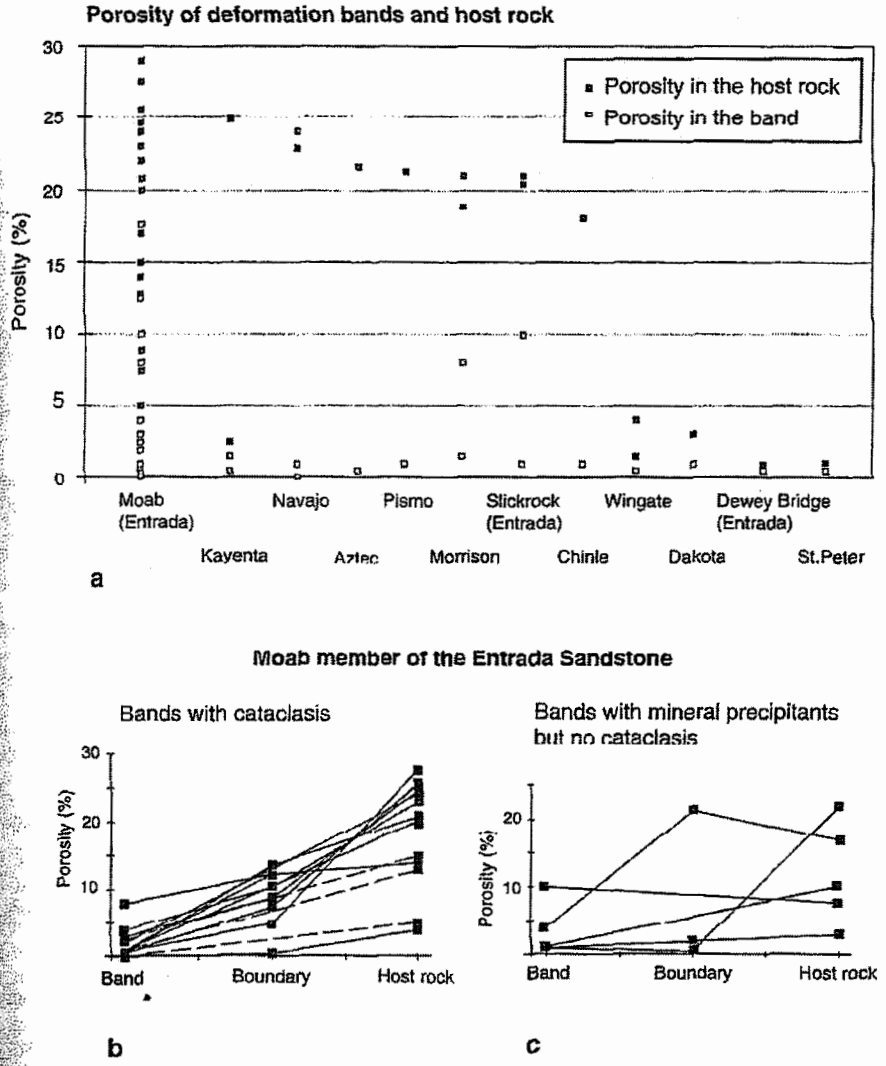

Figure 4—Summary of porosity determinations from image analysis (a) Porosity of deformation bands and host rock in the Moab member of the Entrada Sandstone; (b) bands with cataclasis, (c) bands with mineral precipitants, but no cataclasis. The boundary of a deformation band is defined as an area of damage at the contact between deformation band and host rock. In this area, usually one-half the band thickness, cataclasis and/or pore volume changes are less developed than in the band itself.

section (Antonellini et al., in press). The cataclasis in the bands within the Moab member is developed to different stages; some bands show positive dilatancy, whereas others show compaction. In the latter cases, the pore space of bands may be partially or totally filled with iron oxides, calcite cement, or other diagenetic minerals (Figure 4c). The different microstructures observed in deformation bands of the Moab member can be explained in terms of the host rock porosity and the stress state at the time of their development. Low porosities in the host rock and low confining pressures tend to promote positive dilatancy at early stages, whereas high porosities and high confining pressures tend to promote cataclasis and compaction (Antonellini et al., in press).

The porosity in the wall rock adjacent to well-developed slip planes is very low because of extreme grain crushing and recrystallization. The absolute value of this porosity is below the resolution of the measurement method (< 1%).

Field mapping demonstrates that deformation bands are widely spaced in relatively undisturbed host rock, but exhibit more narrow spacing in proximity to faults. For the purpose of illustrating the

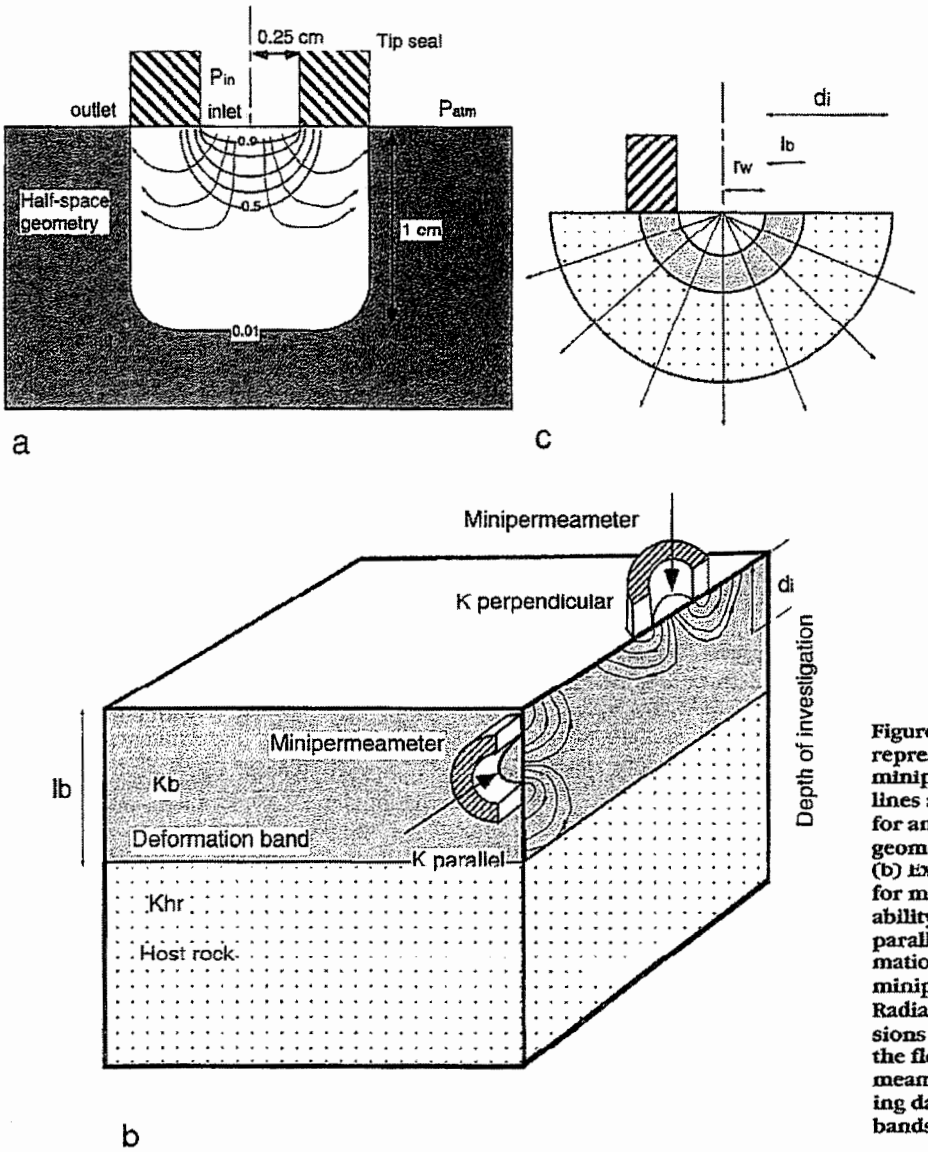

Figure 5—(a) Schematic representation of the minipermeameter. Flow lines and pressure field for an half-space sample geometry are represented. (b) Experimental set-up for measuring the permeability perpendicular and parallel to a zone of deformation bands with the minipermeameter. (c) Radial flow in two-dimensions used to approximate the flow of the minipermeameter when correcting data for deformation bands thinner than 1 cm.

effect of deformation bands on bulk porosity, assume that the number of deformation bands is 100 per meter (a very high value only observed close to some fault zones), the band thickness is 1.5 mm, the porosity in each band is 1%, and the porosity in the host rock is 20%. Using these values, the void loss due to deformation band development would decrease the porosity in 1 m^3 of sandstone only from 20 to 18.5%. Thus, although porosity within bands may have decreased more than one order of magnitude, the bulk porosity of the rock is unlikely to have decreased by more than a few percent. Except in very particular and spatially restricted localities (e.g., in zones adjacent to slip planes), the formation of deformation bands should not seriously compromise the ability of the sandstone to store fluids.

PERMEABILITY

Method

To determine the permeability of a deformation band it is necessary to sample a very small volume of rock. Conventional permeameters (Anderson, 1975) and minipermeameters (Eijpe and Weber, 1971) are designed to perform experiments on core plug samples or on large specimens, and thus are not appropriate for this task. However, some minipermeameters with small diameter tip seals can perform very localized measurements on small volumes of rock (Goggin et al., 1988). These minipermeameters are designed to make rapid, inexpensive, and nondestructive measurements where localized determinations are needed to characterize spatial distribution of permeability in an outcrop or in a core (Goggin et al., 1988).

The minipermeameter used in this study was designed by D. Goggin at Chevron Research Labs and uses gas injection to measure permeability. The flow rate and the pressure drop between injection and atmospheric pressures are measured (Figure 5a). The flow geometry is a function of tip-seal dimensions and sample geometry. These dimensions, together with the measured quantities, can be used in a modified form of Darcy's law (Goggin et al., 1988) to calculate permeability without requiring instrument calibration. Using the numerical solution for an half-space flow geometry, the depth of investigation of a minipermeameter is two times the diameter of the internal tip-seal radius (Goggin et al., 1988). Because the permeameter can operate with an internal tip-seal radius of 0.5 cm, it samples a depth of about 1 cm.

Approximately 600 lab measurements of host rock and deformation-band permeabilities from 48 hand samples were obtained using the permeameter. All samples were unaltered and were selected among a set of 70 specimens collected in the field. Repeated measurements at the same point were taken to test the experimental precision. In low-porosity sandstones (~1.5 md) the measurements had a standard deviation of 0.005 md; in high-porosity sandstones (1500 md) the standard deviation was about 18 md. Samples contained homogeneous zones of deformation bands at least 1 cm thick with no intervening host rock and exposed the material within the deformation band at the surface, on which the tip of the minipermeameter was applied (Figure 5b). Measurements were made on grids (mesh size 1 cm) perpendicular to deformation bands. Permeability was also measured along transects parallel to the zones of bands or at random points on the sample surface.

Four samples had zones of deformation bands with a thickness of less than 1 cm, resulting in a permeability value, obtained with the minipermeameter, that was an average of permeability in the band and in the host rock. For these samples, we needed to apply a correction to estimate the permeability in the direction perpendicular to the band. We did not try to measure the permeability in the direction parallel to the deformation band in these samples.

On the basis of our observations of the microstructure (Antonellini et al., in press) of single deformation bands and of zones of deformation bands with different thickness (0.2–5 cm) we determined that, provided rock properties and genetic conditions are equal, the microstructure is similar regardless of structure thickness. This observation suggests that the permeability also is similar. We also observed that the permeability is affected to a large extent by the low-permeability structures in contact with the minipermeameter tip even if these structures have a very small thickness (~1 mm). This observation suggests the use of a harmonic mean average to correct the measurements. The best match between permeability in zones 1 cm thick and in zones less than 1 cm thick was obtained by correcting the permeability of the latter by approximating the flow geometry of a minipermeameter with that of a radial flow (Dake, 1978) in a plane parallel to the axis of the minipermeameter probe (Figure 5c). In this case, the expression for the harmonic mean permeability becomes

$$\frac{\ln\left(\frac{d_f + r_w}{r_w}\right)}{k_{av}} = \frac{\ln\left(\frac{l_b + r_w}{r_w}\right)}{k_1} + \frac{\ln\left(\frac{d_f + r_w}{l_b + r_w}\right)}{k_2} \qquad (1)$$

In equation 1, k_{av} is the average permeability, k_1 is the permeability perpendicular to the band, k_2 is the permeability of the host rock, r_w is the tip seal internal radius, l_b is the band thickness, and d_f is the depth of investigation. All of the quantities in equation 1 are known by direct measurement on the sample except k_1, the quantity that we are seeking. The two-dimensional radial flow is only an approximation for the actual flow geometry of the minipermeameter. In reality, this flow is donut-shaped rather than radial, and involves gas-compressibility effects neglected in the calculations. Nonetheless, after correction, the values obtained are within a factor of five of those obtained on similar deformation bands in zones at least 1 cm thick. From this comparison, we determined that simple bands with a thickness of 1 mm also have a permeability within a factor of five of values obtained in zones of bands 1 cm in thickness.

Permeability of Deformation Bands

Figure 1 shows the map location of selected samples from Arches National Park. A stratigraphic column for the same region also is used to locate the

samples stratigraphically. The ability to make localized porosity and permeability measurements allows one to make small-scale (centimeter to millimeter scale) profiles of variability. For example, Figure 6 represents a porosity-permeability profile across a single deformation band in the Moab member of the Entrada Sandstone at Delicate Arch Viewpoint in Arches National Park (Figure 1). The porosity in the deformation band drops one order of magnitude and the permeability drops three orders of magnitude in the perpendicular direction from the host rock to the band. Porosity decreases by a factor of three from the host rock to the boundary zone of compaction on either side of the band.

The range of permeability measured in the host rock, parallel and perpendicular to the deformation bands, for the samples collected at Arches National Park is represented in Figure 7. Measurements of permeability in deformation bands with well-developed cataclasis and/or high clay content (samples 2, 47, 49, and 53 from the Moab and Slickrock members of the Entrada Sandstone, and samples 55, b5, and 28 from the Navajo Sandstone in Figure 7) show that the permeability perpendicular to deformation bands is about three orders of magnitude less than in the host rock. Typically, the permeability in the host rock has values of a few darcys, which drops to a few millidarcys or a fraction of a millidarcy in the band.

In the case of samples 39 and 43 (Figure 7), the low permeability perpendicular to the deformation band is not due to cataclasis, but to iron oxide and calcite cement precipitation associated with a dilatant deformation band. This phenomenon occurring along a fault plane is called "diagenetic healing" (Watts, 1987). In another paper (Antonellini et al., in press) we described and discussed these deformation bands that show positive dilatancy (volume increase) in their microstructure instead of cataclasis and compaction. The permeability of a dilatant deformation band in its pristine condition, that means with no iron oxide or cement precipitates, could not be measured.

A sample collected on the western limb of Salt Valley (the sample is similar to samples 39 and 43 in Figure 7) shows a very interesting diagenetic effect that seems to be connected to preferential circulation of fluids within the band. The observed structure is schematically drawn in Figure 8; two bands form an "eye-like" structure which is about 2 cm wide. The increased skeleton porosity within the band is occupied almost completely by iron oxides; a lesser amount of the pore space is free. In the host rock within the eye-like structure the pore space is free or occupied by iron oxides. An 8–10-mm-thick zone of host rock adjacent to the area mineralized with iron oxides shows a total loss of pore space caused by calcite cement precipitation. The calcite cement precipitated in the host rock only in proximity to the band, not within the eye-like structure.

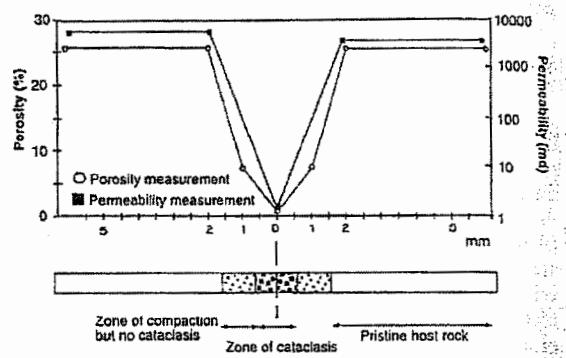

Figure 6—Permeability and porosity profile across a deformation band in the Moab member of the Entrada Sandstone at Delicate Arch Viewpoint.

The spatial distribution of the calcite cement within the host rock and in proximity to the band indicates that the cement precipitated as a result of the interaction between the fluids contained in the host rock and those contained in the band. A temperature increase causes a decrease in solubility of calcium carbonate in solution (Blatt et al., 1980). The presence of iron oxides in the band and of the calcite cement in the adjacent host rock suggests a circulation of hotter mineralizing fluids in the pore space within the band. The interaction of these hot fluids with the water saturating the sandstone may have caused precipitation of the calcite cement in proximity to the band. This sample shows how dilation associated with shearing along a deformation band can affect the fluid circulation and the localization of diagenetic processes in proximity to the bands.

The permeability in deformation bands with precipitants, but no cataclasis (samples 54, 42, and 40 in Figure 7), usually drops less than one order of magnitude with respect to the host rock. This slight reduction in permeability is due to iron oxides and cement precipitation in the increased pore space of a dilatant band.

Figure 9 summarizes the permeabilities measured in the host rock and in the deformation bands, both parallel and perpendicular to the bands. Permeability measured parallel to the deformation bands is usually slightly larger than that measured perpendicular to the deformation band. This difference probably is due to the microfabric of the band. From microstruc-

Figure 7—Permeability in the host rock, parallel and perpendicular to deformation bands, in samples collected at Arches National Park.

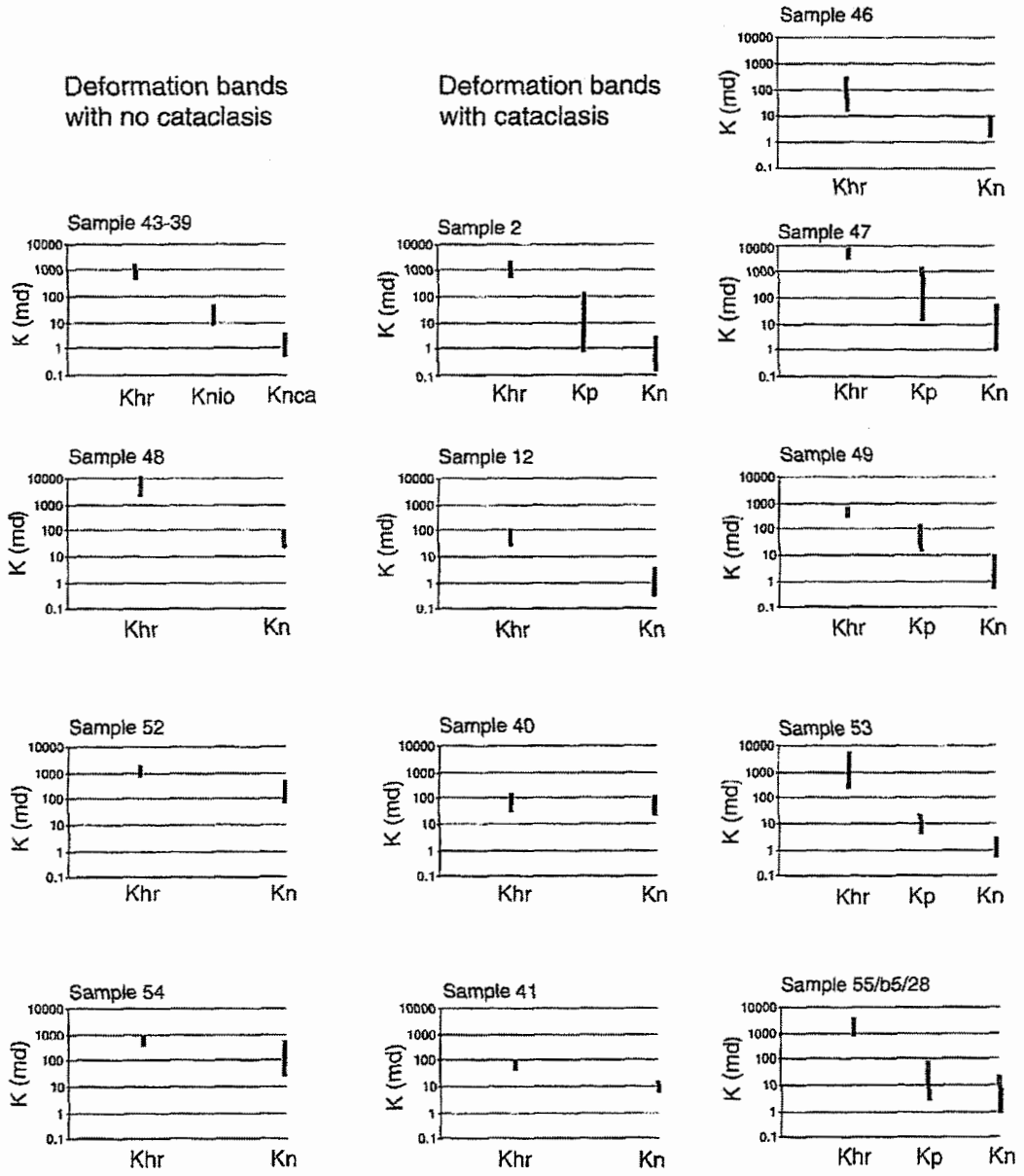

Khr Permeability in the host rock

Kp Permeability parallel to the deformation band

Kn Permeability perpendicular to the deformation band

Knio Permeability perpendicular to the band of iron oxides

Knca Permeability perpendicular to the band of calcite cement

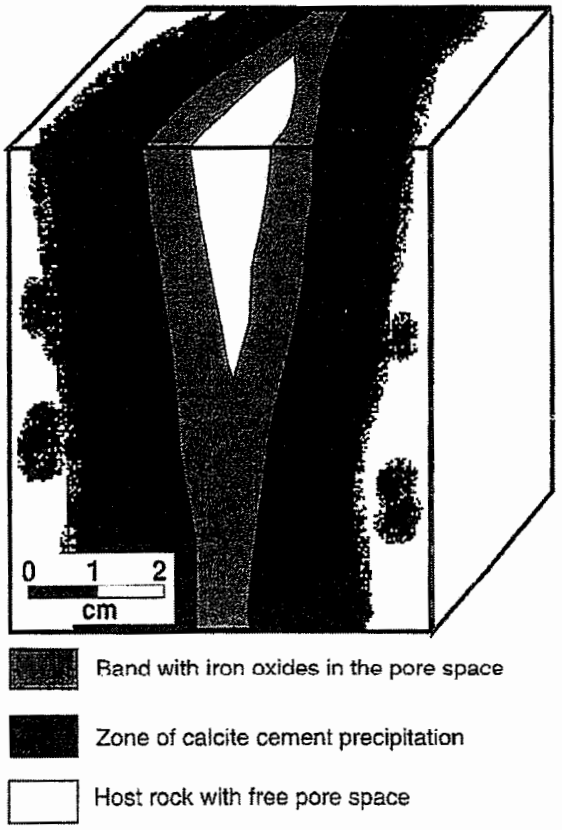

Figure 8—Diagenetic cement precipitation associated with a dilatant deformation band.

tural observations, grains with an oblate shape apparently tend to have their longer axis lying in the plane of the band (Antonellini et al., in press). Within this microfabric, the pores tend to be longer and interconnected in the direction parallel to the band. Interestingly, the largest difference between permeability parallel and perpendicular to a deformation band (one to two orders of magnitude) occurs in the Slickrock member of the Entrada Sandstone. The Slickrock is rich in platy clay minerals (4–15%) that, where compacted in a deformation band, align parallel to it and tend to close any interconnected pore space in the direction perpendicular to the band. The fabric of the clay minerals associated with the compaction in the band and the increased tortuosity perpendicular to a band probably causes the large differential between permeability perpendicular and parallel to a band.

The Moab member of the Entrada Sandstone displays a large variability (over three orders of magnitude) both in host rock and deformation-band permeability (compare the permeabilities of sample 12, 41, and 46 with those of samples 47, 49, and 53 on Figure 7). This variability in permeability reflects the variability in porosity and microstructure already discussed. The deformation bands with lowest permeability are in the clay-rich Slickrock member of the Entrada Sandstone at Arches National Park and in the lower section of the Entrada in the San Raphael Desert (Utah). In this latter unit, the cataclasis is very well developed (Aydin, 1977, 1978; Aydin and Johnson, 1978). By inspecting Figure 9, the largest drop in permeability from host rock to deformation band appears to occur where the permeability of the host rock is largest (e.g., the Navajo, Slickrock, and the

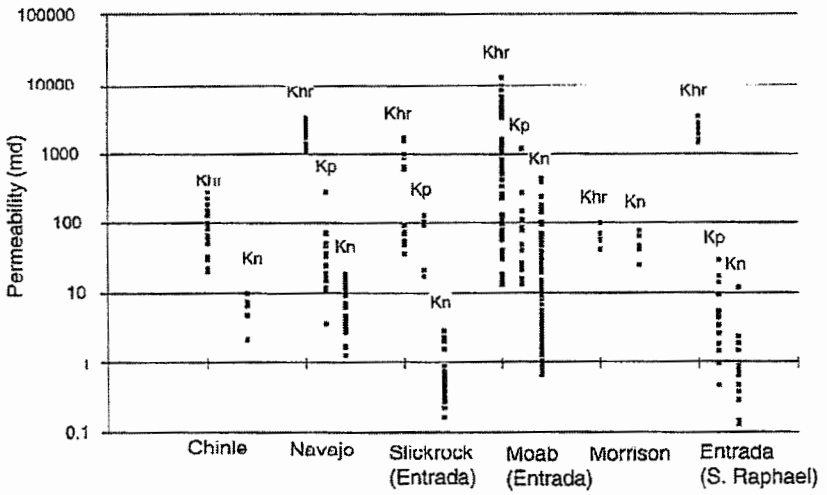

Figure 9—Summary of permeability determinations for deformation bands, Arches National Park and the San Raphael desert.

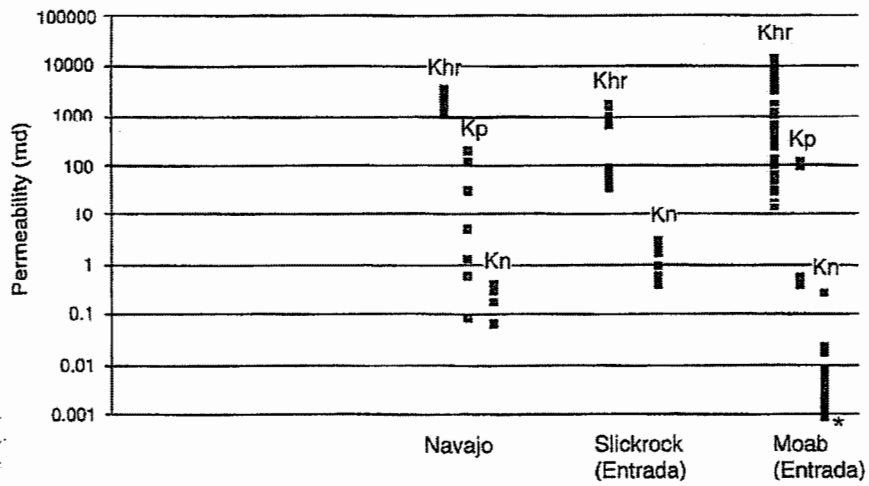

Khr, Kp, Kn Permeability in the host rock, parallel to, and perpendicular to the wall rock of the slip planes

* Limit of instrument detection

Figure 10—Permeability of the wall rock of slip planes at Arches National Park. The lower limit of permeability perpendicular to slip planes in the Moab is not bound because of the limit of the minipermeameter.

Entrada from the San Raphael desert). However, the permeability of deformation bands in rocks where the host rock permeability is already low (~100 md; Chinle and Morrison formations) does not show much lower values (~10–100 md).

Permeability in the Wall Rock of Slip Planes

Permeability was measured in samples from the wall rock of slip planes in the Navajo Sandstone and in the Slickrock and Moab members of the Entrada Sandstone at Arches National Park (Figure 10). The thickness of the wall rock of slip planes ranges from ~ 0.5–6 cm; the permeability was always measured in samples thicker than 1 cm. The permeability measured perpendicular to the wall rock of a slip plane in the Slickrock is comparable to that measured perpendicular to a zone of bands without a slip plane in the same rock type. However, permeability measured perpendicular to the wall rock of a slip plane in the Navajo Sandstone is one to two orders of magnitude less than that of a deformation band and five orders of magnitude less than the host rock.

Wall rocks of slip planes in the Moab member of the Entrada Sandstone at Delicate Arch Viewpoint display the lowest permeability of all samples, with values of less than 0.007 md. This value is only an upper bound, because the experiment had to be terminated after 20 minutes when the flowmeter did not measure a steady flow. The limit of measurement of the permeameter appears to be greater than the permeability of the sample. The permeability perpendicular to these zones adjacent to slip planes is at least seven orders of magnitude less than that in the pristine host rock. Wall rocks adjacent to slip planes have extremely low porosity, extensive cataclasis, and recrystallization, causing the most conspicuous drop in permeability within the porous sandstones investigated in this study.

PORE NETWORK STRUCTURE AND SEALING PROPERTIES

The sealing properties of a rock are determined by the minimum pressure required for a nonwetting phase, such as a hydrocarbon, to displace the connate water out of the pore space (Hubbert, 1953; Schowalter, 1979; Downey, 1984). This minimum pressure is the capillary pressure (P_c) of the rock. The capillary pressure depends on the radius of the interconnected pore space (R), interfacial tension (γ), and wettability (θ) according to the relationship (Purcell, 1949):

$$P_c = \frac{2\gamma \cos\theta}{R} \qquad (2)$$

which is illustrated in Figure 11a. This same relation was expressed in terms of average grain diameter (d)

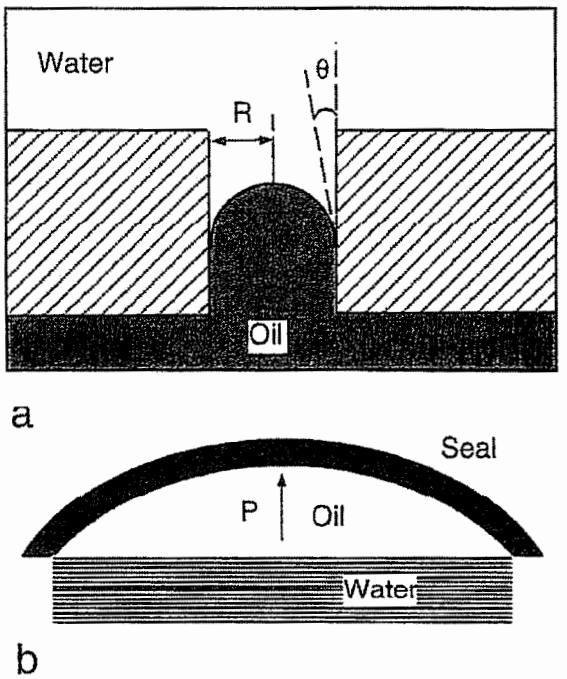

Figure 11—Definitions of wettability; (a) pore radius and (b) hydrocarbon displacement pressure.

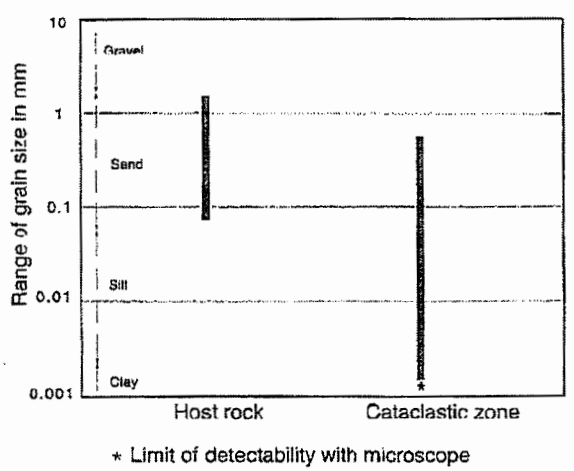

Figure 12—Range in grain size in the host rock and in the cataclastic zone. The fields of grain sizes for gravel, sand, silt, and clay are given by the arrows.

and a dimensionless factor of proportionality, C, by Hubbert (1953):

$$P_c = \frac{C\gamma \cos\theta}{d} \tag{3}$$

The capillary pressure may seal a column of hydrocarbons exerting an equivalent or lesser pressure (Figure 11b). The hydrocarbon pressure (P) arises from buoyancy forces and is given by the relation:

$$P - (\rho_w - \rho_{ho})gh \tag{4}$$

where ρ_w is the density of the water, ρ_{ho} is the density of the hydrocarbon, g is the acceleration of gravity, and h is the height of the hydrocarbon column. A seal is broken when $P > P_c$. The wettability, θ, and specific properties of the hydrocarbon, such as γ and ρ_{ho}, are not discussed here. For the purposes of this paper, the most relevant factor controlling capillary pressure is the effective interconnected pore radius R; the smaller the radius, the larger the capillary pressure. Capillary pressures, as shown by equation 2 or 3, do not depend on seal thickness. Of course, seal quality cannot be evaluated simply on microproperties, such as interconnectedness of the pore space; one must also consider macroproperties, such as lateral continuity, thickness, and ductility (Downey, 1984; Grunau, 1987). We consider the microproperties of seals in sandstone in this paper and will address the macroproperties in another paper (Antonellini and Aydin, in preparation).

Grain size within a deformation band may be one to two orders of magnitude smaller than in the host rock (Figure 12). The minimum grain size in a band can easily drop into the clay-size range (<0.004 mm). According to Hubbert's (1953) equation 3 and the grain-size data for deformation bands at Arches National Park, capillary pressure within a deformation band probably will be 10 to 100 times larger than in the host rock. Pittman (1981) presented mercury injection curves on core plugs from fault zones in porous sandstones (Simpson Group, Oklahoma). These curves show a wide distribution in pore aperture sizes. Nevertheless, these data are interesting because they also show that pore aperture sizes can be one to two orders of magnitude less than those in the undeformed host rock.

Image analysis was used in our study to characterize pore network geometry and its interconnectedness within a deformation band. An algorithm called the Fast Montoto Transform (Montoto, 1982; Quinn, 1988) can be applied to the analysis of video camera thin-section images to visualize the skeleton and the width of the interconnected pore space. This image processing technique starts from a segmented image of a thin section. Through a process of thickening/thinning, similar

to the process of erosion/dilation commonly used in image analysis (Full et al., 1984; Ehrlich et al., 1985), one can obtain the skeleton of the interconnected pore space.

In Figure 13a and b some of these transforms are calculated for bands with cataclasis. These images are only two-dimensional representations (thin sections) of rocks; however, their structure can be used to extrapolate to the three-dimensional arrangement of the pore network. The interconnected pore space obviously is better developed in the host rock (range of length: 0.0026-0.5 mm) than in the band (range of length: 0.0026–0.092 mm). Within the bands, the interconnected pore space is shorter and more fragmented (Figure 13a, b). The pore network tends to be isotropically distributed in the host rock, whereas in the band the pore network is preferentially developed in a direction parallel to the deformation band. This fabric of the pore space within the band is probably caused by the grains with an oblate shape that tend to align with their long axis parallel to the plane of the deformation band. The pore space is not widely extended in the direction perpendicular to the band and we observed no connections from one side of a band to the other (Figure 13).

The minimum width of the pore space resolvable with the image analysis system employed is about 0.3–0.5 μm. If interconnected pore space exists perpendicular to a deformation band, it should have an effective width less than or equal to these values. By substituting these values into equation 2 and using 25 dynes/cm for the expression $\gamma \cos \theta$ (a typical value for a hydrocarbon; Hubbert, 1953), one obtains a capillary pressure of 1.66×10^5 Pa. This pressure is equivalent to a hydrocarbon column of 64 m, using a typical value of 2.26 kPa/m as a differential in pressure between hydrocarbon and water (Zieglar, 1992). Given the difficulty of checking the effective three-dimensional interconnectedness of the pore space from a two-dimensional image, we consider this value an upper boundary. However, if we assume that the capillary pressure in a deformation band has the potential to seal a hydrocarbon column about 64 m in height, effective sealing clearly depends on the verti-

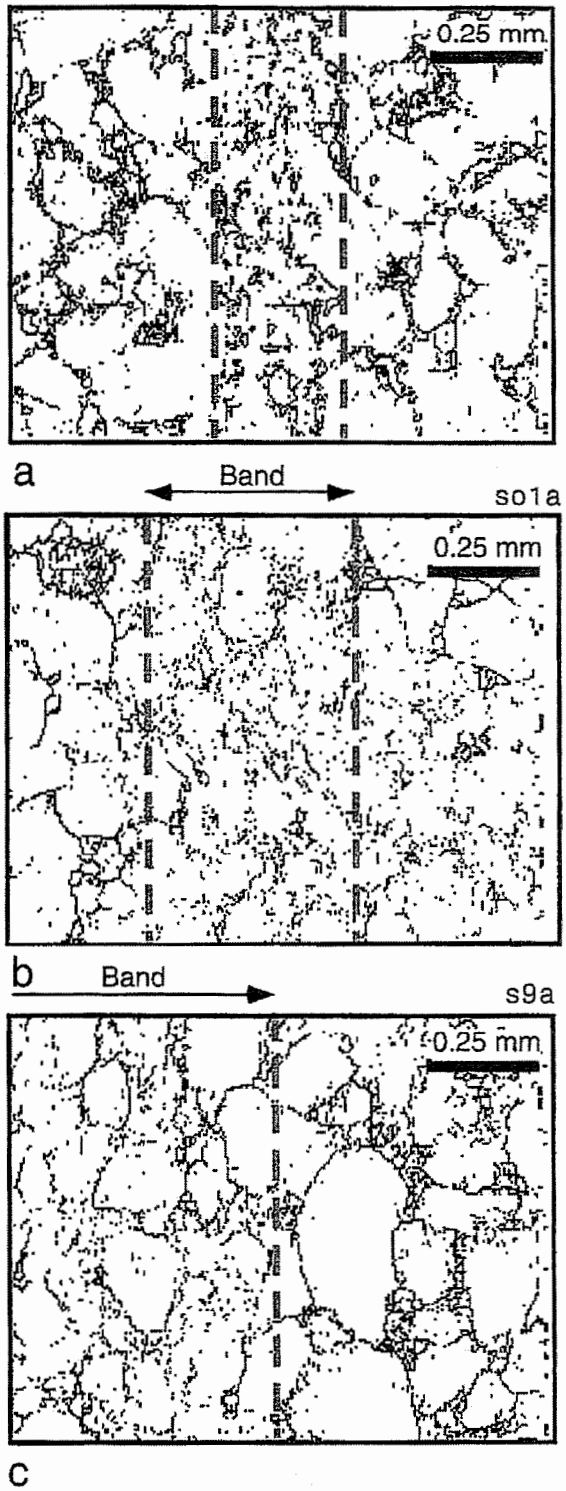

Figure 13—Interconnected pore space of deformation bands and host rock represented with the Fast Montoto Transform. Note the fragmentation of the interconnected pore space in the bands and its tendency to align parallel to the direction of the deformation bands. (a) Deformation band in the Moab member of the Entrada Sandstone at Delicate Arch Viewpoint. Cataclasis is well developed. (b) Deformation band from the Garden area (Arches National Park). (c) Deformation band from the Delicate Arch Viewpoint area. Band of compaction only and little or no cataclasis.

cal and lateral continuity of this structure.

Estimates of the capillary pressure of deformation bands also can be made using grain size and the relation given by Hubbert (1953), the equations proposed by Berg (1975) and Pittman (1992) that relate porosity and permeability to capillary pressure, or even by direct measurement of pore sizes from image analysis. Using equation 3 and grain sizes typical of a deformation band (Figure 12), one would get estimates for the capillary pressure ranging from 3 to 45 m of an equivalent hydrocarbon column. Hubbert's (1953) relation is for a homogeneous grain size; the wide grain size distribution in a band would probably lower pore throat interconnectedness and would potentially increase the capillary pressure with respect to these values. Using pore width (Figure 14) and the relation 2 proposed by Purcell (1949), one would obtain an estimate for the capillary pressure ranging from 2.3 to 40 m. Using Berg's empirical formulas (1975) relating permeability and porosity to capillary pressure, one would obtain a range in values for the latter between 3 and 50 m of an equivalent column of hydrocarbons.

Pittman's empirical formulas (1992) were used to determine the displacement pressure of the bands. The displacement pressure is the pressure necessary to have an interconnected filament of hydrocarbon through the largest connected pore space, which by convention corresponds to 10% mercury saturation (Pittman, 1992). These relations indicate displacement pressures on the order of 100–150 m of an equivalent hydrocarbon column. The parameters used in these formulas were typical for a deformation band in the Moab member of the Entrada Sandstone at Delicate Arch Viewpoint: 2–3% porosity and permeabilities on the order of 1–2 md. The estimates provided by this analysis are meant to constrain the order of magnitude of the range of capillary pressures in a deformation band.

The pore network geometry of a band with no cataclasis and only compaction is represented in Figure 13c for the Moab member of the Entrada Sandstone. The pore network within the band is less developed than that in the host rock; however, it still shows an isotropic pattern and a certain degree of interconnectedness. In this kind of band, the permeability is reduced about one order of magnitude with respect to the host rock (samples 52 and 54 in Figure 7).

Figure 14 is a plot of pore diameter determined from image analysis versus the cumulative percent of pore space for a deformation band and the corresponding host rock. This diagram does not represent the effective interconnected diameter of the pore space (as would be obtained from a mercury injection curve), but only pore space size and frequency as it appears from image analysis. Regardless of this limitation, the curve is interesting because it shows

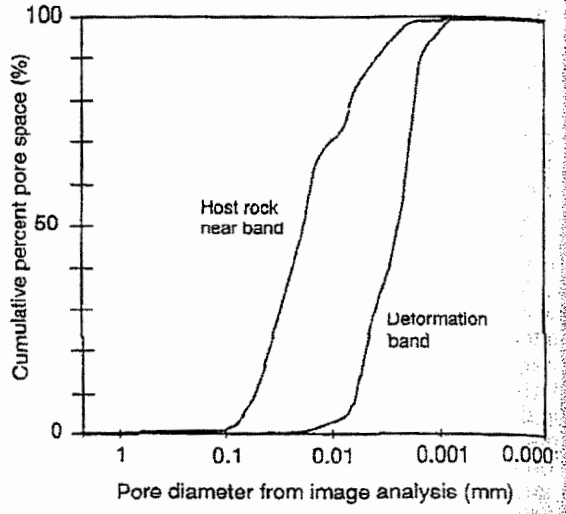

Figure 14—Pore-throat diameter distributions from image analysis versus cumulative percent of pore space. Pore space within a deformation band is one to two orders of magnitude smaller than in the host rock near the deformation band.

that the pore space within a deformation band is one to two orders of magnitude smaller than that in the surrounding host rock. The curve also shows that the distribution of pore diameters is relatively narrow (steep slope), a very different result from the wide distribution of effective pore radii measured by Pittman (1981) with mercury injection. The narrow distribution in Figure 14 points out that the pore radii within a deformation band are quite uniform and of small size; however, when comparing these diagrams, one has to consider that only pore size, and not the effective pore diameter, can be measured from image analysis and that the limit of pore size detection is about 0.3–0.5 μm.

Effective sealing and compartmentalization caused by zones of deformation bands with respect to hydrocarbon migration in a sandstone reservoir is evident in outcrop at Pismo Beach in central California. Figure 15 is a photograph of an outcrop in the Miocene–Pliocene Pismo Formation; the zones of deformation bands isolate compartments 2 to 10 m wide, some of which are saturated by hydrocarbon (tar). Zones of deformation bands act as seals and bound tar-impregnated rock from tar-free sandstone.

Provided lateral and vertical continuity exists, relatively thin (millimeter to centimeter) deformation bands can be very efficient in sealing small columns of hydrocarbons, such as those in turbiditic and channel

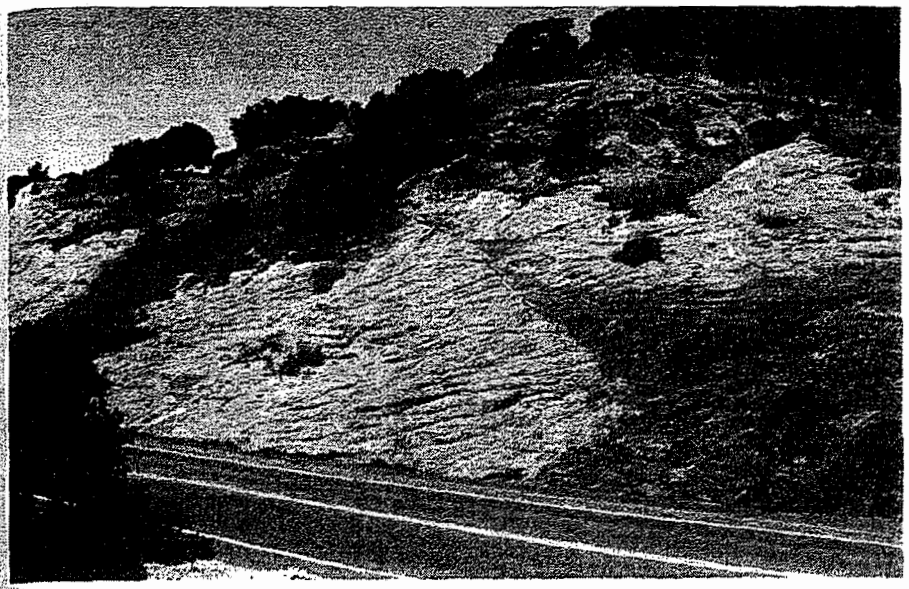

Figure 15—Photograph of the road cut on Price Canyon road near Pismo Beach, central California. The deformation bands isolate compartments saturated with hydrocarbons (tar) from compartments not hydrocarbon saturated.

deposit reservoirs, or where the gravity of the oil is high. The wall rocks of slip planes probably have capillary pressures much higher than those of a single deformation band because of extreme compaction and recrystallization, but how much higher cannot be quantified from image analysis with precision.

PERMEABILITY OF FAULT ZONES IN SANDSTONE

Faults with offset larger than a few meters commonly are associated with a variety of structures (joints, deformation bands, slip surfaces, gouge or breccia zones, etc.); we define the ensemble of these structures as a fault zone. In sandstone, fault zones may consist of multiple slip plane segments associated with zones of deformation bands in a complex three-dimensional arrangement.

The ability to evaluate fault zone permeability is of strategic importance when planning the development of a reservoir or when evaluating sealing or preferential paths for fluid migration. Previous work on this topic is very scarce in the literature and exists only at the qualitative level. Maclay and Small (1983) and Kastning (1977) investigated positive and negative influences of fault zones on permeability in carbonate rocks. Kastning (1977) and Nelson (1985) concluded that faults either may enhance or decrease permeability depending on whether the faults are associated with fracturing or with mineral precipitation in the fault plane. Fluid flow along fault zones at a crustal and regional scale has been addressed by McCaig (1989), Knipe et al. (1991), Logan (1991), Moore et al. (1991), Rice (1992), and Sleep and Blanpied (1992), and the effect of confining pressure and shear stress on fault gouge permeability has been discussed by Teufel (1981), Shi et al. (1980), and Morrow et al. (1984). These latter authors conducted lab experiments and noted a decrease in permeability with increasing confining pressure and shear stress. The decrease in permeability was accentuated if the grain size of the gouge was coarse rather than fine.

Smith (1980), Pittman (1981), Seeburger (1981), and Seeburger et al. (1991) considered fault zones in sandstone and suggested that permeability perpendicular to fault zones is decreased by granulation and cataclasis, whereas permeability parallel to the fault zone is enhanced along the slip plane discontinuity. This enhancement of fluid migration parallel to slip planes also has been reported by Secor (1965) and Weber and Daukoru (1975); however, Downey (1984) warned that this phenomenon may be developed only in faults at shallow depths, because confining pressure tends to hold fault plane surfaces and fractures shut at greater depth. Finally, Bernard et al. (1989) numerically investigated permeability anisotropy induced by a fault zone in an aquifer.

In this paper, we attempted to quantify permeability of a fault zone in sandstone by combining detailed field mapping at different scales and data from minipermeameter measurements. We believe that fault zone permeability can be evaluated only if

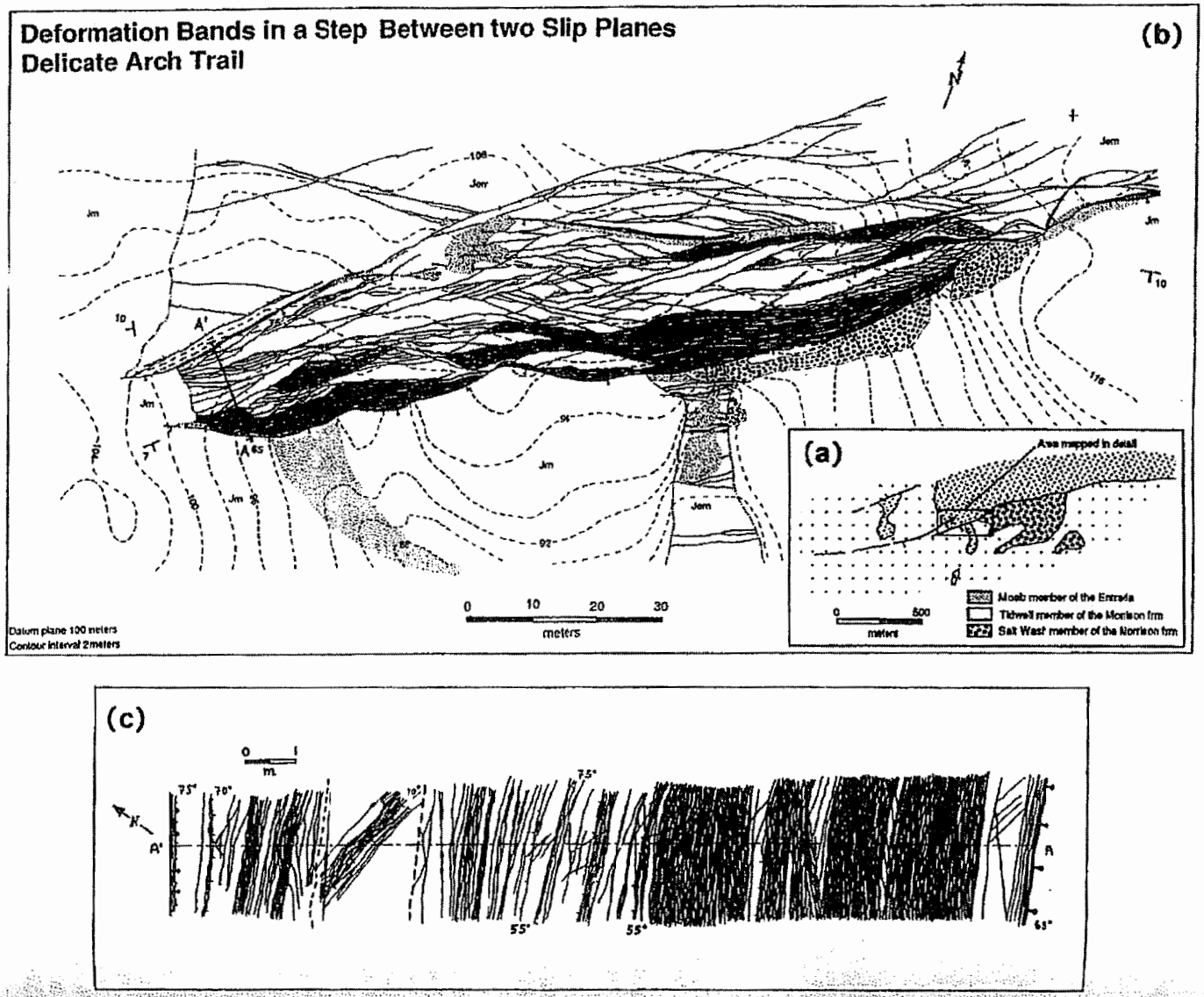

Figure 16—Step between two slip planes along the Delicate Arch Trail. (a) Location of the map for b. (b) Detailed map of the step. Slip planes have a dot on their down-thrown side, whereas deformation bands have a dash on their down-thrown side. (c) String map along the transect AA' in b.

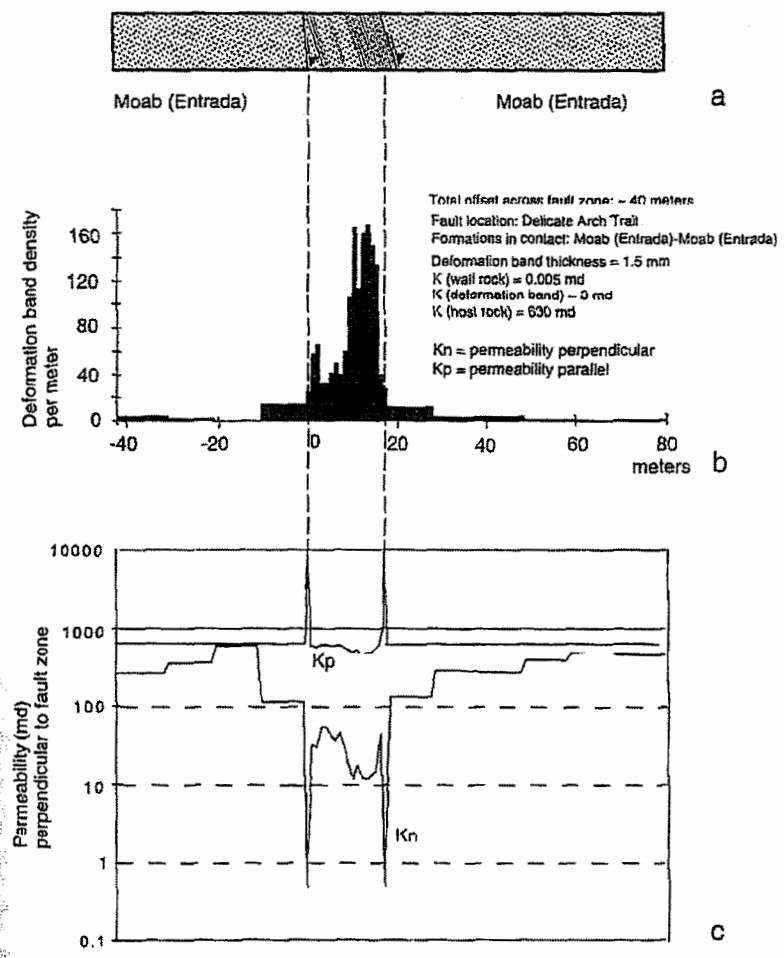

Figure 17—Permeability across the transect AA' measured in Figure 16c. (a) Schematic cross section across the fault zone. (b) The histogram shows the number of deformation bands per meter. (c) Calculation of the average permeability over the distance of 1 m.

realistic values of the petrophysical properties of various structural elements making up the fault zone are provided and if all the geometric characteristics of the fault zone are known. We illustrate this method using a case study from the Delicate Arch area at Arches National Park.

Case Study

Detailed geologic mapping at various scales was employed to document fault structure and deformation band distribution in the Moab member of the Entrada Sandstone. Slip planes and zones of deformation bands were mapped at a scale of 1:4000 on a base of aerial photographs; the map of an array of these slip planes is given in Figure 16a. The traces of the slip planes are characteristically segmented forming steps at various scales. The detailed geometry of these segments is described in Antonellini and Aydin (in preparation). A map at a scale of 1:250 was made of a step between two slip plane segments using an electric distance meter (EDM)-equipped theodolite (Figure 16b, particularly detail of the area within the rectangle in Figure 16a). The map shows the anastomosing and interconnected pattern of the deformation bands and zones of deformation bands, and the stepping geometry of the slip planes. This normal fault zone has an offset of about 30–40 m. To the west, this sandstone unit is overlain by the shaly deposits of the Morrison Formation. The deformation mechanism in this member of the Morrison Formation is completely dif-

ferent from that in the underlying sandstone and consists of drape folding. The increase in density of deformation bands in proximity to the fault zone is similar to that reported by Jamison and Stearns (1982) in the Colorado National Monument.

A transect along line AA' was string-mapped (scale 1:45) to determine the distribution of deformation bands (Figure 16c). A photographic mosaic was taken along the trace of the transect and of its southern and northern extensions. Deformation band density per meter was measured on the photographic mosaic (Figure 16c). The results are plotted in a histogram in Figure 17b. Samples were collected along this transect, and permeability was measured in the lab with the minipermeameter to characterize the hydraulic properties of the structural elements.

At this point, all the relevant geometric and petrophysical parameters of interest along the transect are known: deformation band thickness, thickness of the cataclastic wall rock adjacent to slip planes, deformation band density, deformation band permeability, host rock permeability, and permeability of the wall rock of slip planes. By measuring permeability perpendicular and parallel to the deformation bands (Figure 18) and the wall rock of the slip planes (assumed to be the principal axes of permeability), we can determine the anisotropic permeability tensor within these structures. From this, the permeability in any direction can be calculated. For example, the horizontal component of permeability across the fault plane (which is of interest in a medium with horizontal layers where the flow is bedding-parallel) can be calculated from the anisotropic permeability tensor after coordinate rotation of an angle 90 − α, according to the formula:

$$K_{ij}^{new} = A^T K_{ij}^{old} A \qquad (5)$$

where α is the amount of dip of the fault plane (to be used in the matrix of director cosines), K_{ij} is the anisotropic permeability tensor, and A is the matrix of director cosines (Malvern, 1969).

The average horizontal permeability in the fault zone over the scale of interest can be evaluated by taking the permeability harmonic mean, according to the relation (Deutsch, 1989):

$$k_{av} = \frac{k_h k_b k_s L}{(k_b k_s) l_h + (k_h k_s) l_b + (k_h k_b) l_s} \qquad (6)$$

where k_{av} is the average permeability over the distance L; and k_h, k_b, and k_s are the permeabilities of the host rock, of the deformation bands, and of the wall rock of the slip plane, respectively. The total thicknesses of the host rock, the deformation bands, and the wall rock of the slip plane are respectively l_h, l_b, and l_s. The results of the calculation for horizontal

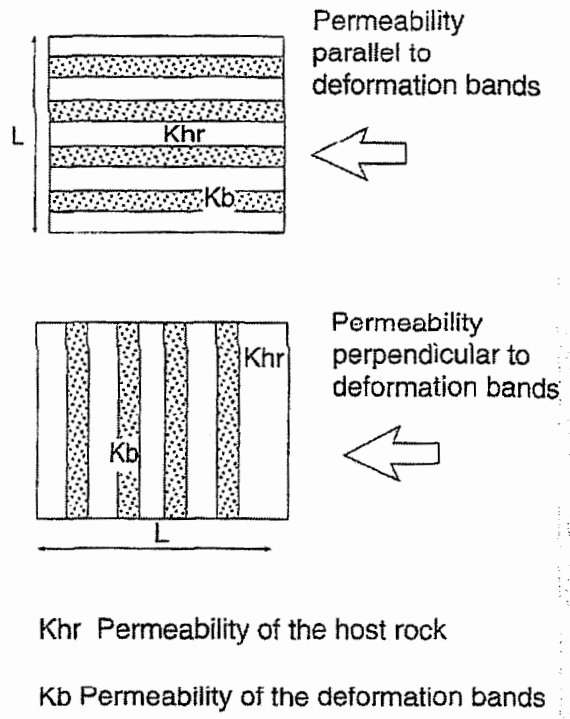

Figure 18—Two different ways of averaging permeability: in parallel (Kp) and in a series (Kn).

permeability (almost perpendicular to the fault trace) is shown in Figure 17c, together with the measured values of the permeability and the structural element thickness used for the case under consideration.

Over the length scale of 1 m, the largest negative anomaly in permeability is caused by the wall rock of slip planes. Although thicknesses of low-permeability zones adjacent to slip planes are very small (~1 cm), the effect of their low permeability has a strong impact over a large scale. Figure 19a shows this effect; here, the average permeability has been calculated over length scales of 1, 10, 20, and 40 m for the same transect. This analysis shows the effective influence of low-permeability fault zones on blocks of different sizes as they may be implemented in a reservoir simulation numerical model. The permeability anomaly of a fault zone has to be considered at the scale length of the problem to solve. If the scale length is small, the anomaly is very large; if the scale length is large, the anomaly is relatively less important.

Figure 19c shows the permeability profile across the fault zone without considering the effect of the wall rocks of the slip planes. At the scale length of 1 m, the permeability drops only one to two orders of

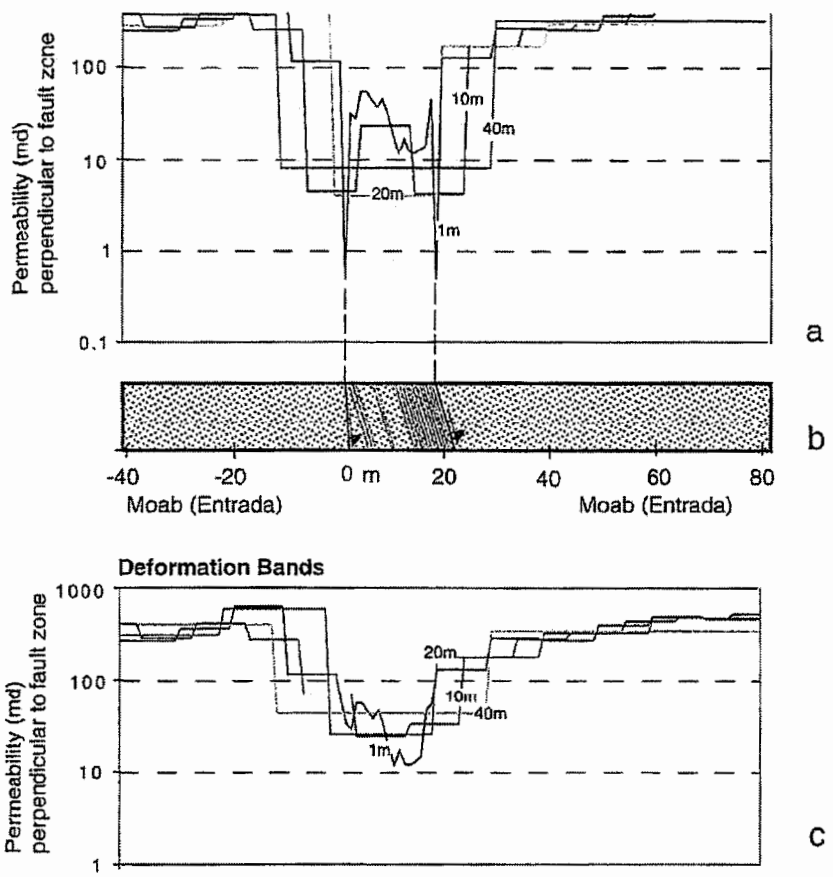

Figure 19—Permeability variations across the fault zone at different scales. (a) The harmonic mean permeability is calculated for blocks of different length for the fault zone of Figure 18. (b) Schematic cross section of the fault zone. (c) Permeability profile as in (a), but without considering the effect of the slip planes.

magnitude in the fault zone with respect to the host rock; however, if one considers the effect of the wall rock, it drops three orders of magnitude. This is interesting because slip planes are not laterally continuous along a fault zone (Antonellini et al., in preparation), but instead tend to step (Figure 16). In a step, the fluids may circulate around the slip plane and encounter only the deformation bands; therefore steps between slip planes can represent relatively less impervious paths for fluid migration perpendicular to the fault zone.

During the field study, it was often possible to observe iron oxides, manganese, or calcite cement along slip planes at several localities within Arches National Park. In particular, along northwest-southeast-trending faults in the northern part of the salt anticline (east of the Rock Corral area), it is very common to find a 10–15-cm-thick zone of mineralization in the opening at the contact between the slip plane and rocks of the hanging wall (Figure 20). Here, the fault separates the Navajo Sandstone in the footwall from the Cedar Mountain Formation in the hanging wall; the offset across this fault is about 400–500 m. The mineralization consists of large (2–3 mm), equant calcite crystals with almost no impurities and no pore space.

The mineral precipitates along fault planes can be considered evidence for preferential fluid circulation parallel to the fault zone; however, its real quantification in terms of conductivity and its eventual variability with depth under the influence of confining pressure cannot be assessed by the field study alone.

Figure 17c presents a calculation of the permeability parallel to the fault zone in the case study. The effect of the deformation bands on parallel flow can be calculated by arithmetic mean according to this formula (Deutsch 1989):

$$k_{av} = \frac{k_h l_h + k_b l_b + k_s l_s}{L} \qquad (7)$$

where k_{av} is the average permeability over the distance L; k_h, k_b, and k_s are the permeabilities of the

Figure 20—Photograph of calcite mineralization at the contact between slip plane and hanging-wall rock. The fault is in the northern part of Salt Valley, east of the Rock Corral area. The chisel is 20 cm long.

host rock, deformation bands, and wall rock of the slip plane, respectively. The total thicknesses of the host rock, deformation bands, and wall rock of the slip plane are l_h, l_b, and l_s, respectively. The decrease in permeability apparently caused by the deformation bands is less than a factor of 2 with respect to the permeability of the host rock and, therefore, it is negligible also where the bands are narrowly spaced.

The permeability along the discontinuity represented by the slip plane may be very high because of the unboundedness of the slip-plane surfaces and the opening between them. The value for slip-plane–discontinuity parallel permeability is hypothetical and is meant only to represent the contrast with respect to the flow perpendicular to the fault zone (Figure 17c).

Fault Zones in Different Sandstone Types

Several transects across fault zones in various rock types, as well as between different rock types, have been mapped and the harmonic mean permeability per meter in the direction perpendicular to the fault zone has been calculated. The results are shown in Figure 21. In all these diagrams, one can clearly see that the largest permeability anomaly is associated with thin zones of cataclastic and recrystallized wall rock of slip planes. This anomaly persists regardless of the fact that the thickness of the wall rock of slip planes is always very limited (0.5–5 cm) compared to the length over which the permeability is averaged (1 m).

In general, deformation bands within the fault zones (Figure 21) decrease the permeability of 1 m^3 of sandstone by about one to one and one-half orders of magnitude. The cataclastic wall rock of the slip planes, however, may decrease permeability about three orders of magnitude. The transect in Figure 21a shows a fault zone in the Navajo Sandstone that is very similar to the one previously described in the Moab member of the Entrada Sandstone along the Delicate Arch trail (Figure 16). In Figure 21a there are also two slip planes bounding a zone of high deformation band density; the decrease in permeability perpendicular to the fault zones is similar to that observed in Figure 17c within the step along the Delicate Arch trail (approximately three orders of magnitude over this scale length).

CONCLUSIONS

Experimental and field evidence suggest that fluid flow properties of a sandstone can be affected by cataclasis and porosity changes in fault zones. Faulting in sandstone may be as simple as a single deformation band or as complicated as a fault zone with several slip planes and anastomosing zones of deformation bands in a complex three-dimensional geometry.

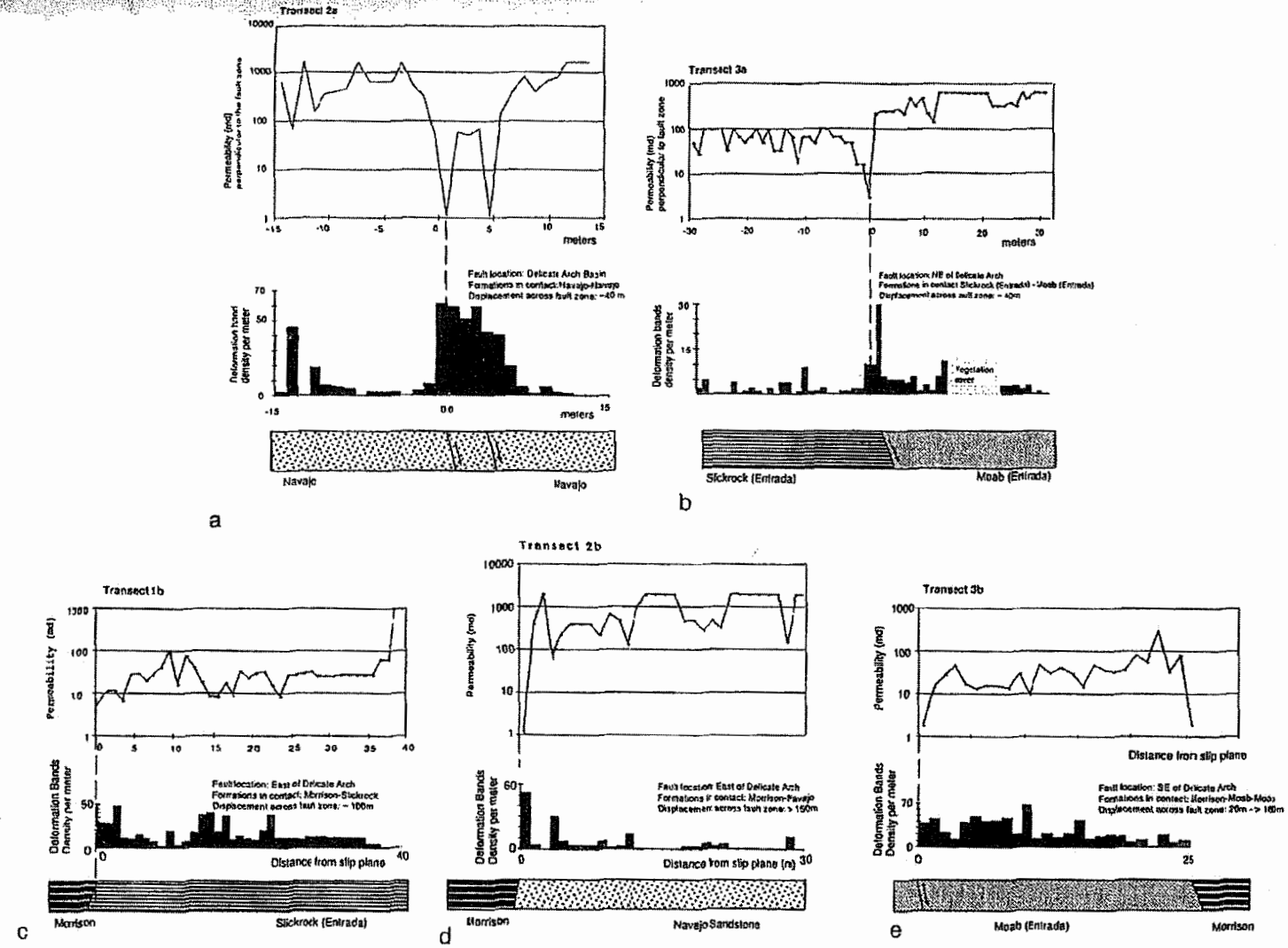

Figure 21—Number of deformation bands per meter and relative permeability profiles across fault zones among different rock types. See Figure 1 for the locations of the transects.

Porosity in a single deformation band drops about one order of magnitude with respect to that of the host rock, whereas in the cataclastic wall rock of a slip plane, porosity is practically absent. The larger the porosity in the pristine host rock, the lower the porosity in the deformation band. Porosity in a deformation band decreases where cataclasis is well developed (a compacted band), but may increase if cataclasis is absent (a dilatant band). Because of their localized nature, deformation-band and fault-zone porosity loss does not generally affect the storage property of a porous sandstone at a reservoir scale.

The permeability of a fault zone can be significantly different from the permeability of the surrounding host rock. Deformation bands have permeabilities of one to four orders of magnitude less than the surrounding rock (on average, about three orders of magnitude less). An increasing amount of cataclasis in the band and a significant clay content in the host rock promote permeability reduction in the deformation bands. Permeability parallel to a deformation band is usually about one order of magnitude larger than that perpendicular to the deformation bands, especially when the band contains grains having an oblate shape. The largest permeability drop between deformation bands and the associated host rock occurs where the porosity of the pristine host rock is largest. Permeability can be a highly variable quantity even within the same rock unit, as demonstrably the case of the Moab member of the Entrada Sandstone.

The cataclastic and recrystallized wall rocks of slip planes have permeabilities as low as seven orders of magnitude less than that in the pristine host rock. These relatively low values have a strong effect on the permeabilities in the direction perpendicular to a fault zone at different scales of interest. However, qualitative observations of fault plane mineralization suggest a preferential path for the fluids along the discontinuity defined by the two surfaces of a slip plane.

The pore network geometry of deformation bands is extremely fragmented and anisotropic in the plane parallel to the band. By measuring grain sizes and pore apertures, and by inference from image analysis, it is possible to constrain the capillary pressure within a deformation band. The calculated values for the capillary pressure range from a few meters to about 100 m of an equivalent column of hydrocarbons if cataclasis is well developed. Deformation bands, zones of deformation bands and the wall rock of slip planes have potentially good sealing properties, as confirmed by field examples. However, the petrophysical properties of a fault zone cannot by themselves characterize sealing and fluid flow in a reservoir. One must consider the lateral and vertical variations of these properties, which are directly related to geometry and structure of slip planes and deformation bands.

REFERENCES CITED

Anderson, G., 1975, Coring and core analysis handbook: Tulsa, Oklahoma, PennWell, 200 p.

Antonellini, M. A., A. Aydin, and D. D. Pollard, in press, Microstructure of deformation bands in porous sandstones at Arches National Park, Grand County, Utah: Journal of Structural Geology.

Aydin, A., 1977, Faulting in sandstone: Ph.D. thesis, Stanford University, Stanford, California, 282 p.

Aydin, A., 1978, Small faults formed as deformation bands in sandstone: Pure and Applied Geophysics, v. 116, p. 913–930.

Aydin, A., and A. M. Johnson, 1978, Development of faults as zones of deformation bands and as slip surfaces in sandstone: Pure and Applied Geophysics, v. 116, p. 931–942.

Aydin, A., and A. M. Johnson, 1983, Analysis of faulting in porous sandstones: Journal of Structural Geology, v. 5, p. 19–31.

Berg, R. R., 1975, Capillary pressures in stratigraphic traps: AAPG Bulletin, v. 59, p. 939–956.

Bernard, D., M. Danis, and M. Quintard, 1989, Effects of permeability anisotropy and throw on the transmissivity in the vicinity of a fault: American Geophysical Union, Geophysical Monographs, v. 47, p. 119–128.

Bevan, T. G., 1985, Tectonic evolution of the Isle of Wight: a Cenozoic stress history based on mesofractures: Proceedings Geological Association, v. 96, p. 227–235.

Blatt, H., G. Middleton, and R. Murray, 1980, Origin of sedimentary rocks: Englewood Cliffs, New Jersey, Prentice-Hall, 634 p.

Bouvier, J. D., K. Sijpesteijn, D. F. Kluesner, C. C. Onyejekwe, and R. C. Van der Pal, 1989, Three-dimensional seismic interpretation and fault sealing investigations, Nun River field, Nigeria: AAPG Bulletin, v. 73, p. 1397–1414.

Dake, L. P., 1978, Fundamentals of reservoir engineering: Amsterdam, Elsevier, 443 p.

Deutsch, C., 1989, Calculating effective absolute permeability in sandstone/shale sequences: SPE Formation Evaluation, v. 4, p. 343–348.

Doelling, H., 1985, Geology of Arches National Park: Utah Geological and Mineral Survey, no. 74, 15 p.

Downey, M. W., 1984, Evaluating seals for hydrocarbon accumulations: AAPG Bulletin, v. 68, p. 1752–1763.

Ehrlich R., S. J. Crabtree, S. K. Kennedy, and R. L. Cannon, 1985, Direct estimation of flow properties from petrographic thin section image analysis, *in* W. C. Park, D. M. Hausen, and R. D. Hagni, eds., Applied mineralogy: Los Angeles, American Institute of Mineralogy, p. 205–221.

Eijpe, R., and K. J. Weber, 1971, Mini-permeameters for consolidated rock and unconsolidated sand: AAPG Bulletin, v. 55, p. 307–309.

Engelder, J. T., 1974, Cataclasis and the generation of fault gouge: Geological Society of America Bulletin, v. 85, p. 1515–1522.

Full, W. E., R. Ehrlich, and S. K. Kennedy, 1984, Optimal configuration and information content of sets of frequency distributions: Journal of Sedimentary Petrology, v. 54, p. 117–126.

Goggin, D. J., R. L. Thrasher, and L. W. Lake, 1988, A theoretical and experimental analysis of minipermeameter response including gas slippage and high velocity flow effects: In Situ v. 12, p. 79–116.

Grunau, H. R., 1987, A worldwide look at the cap-rock problem: Journal of Petroleum Geology, v. 10, p. 245–266.

Harding, T. P., and A. C. Tuminas, 1988, Interpretation of footwall (low side) fault traps sealed by reverse faults and convergent wrench faults: AAPG Bulletin, v. 72, p. 738–757.

Hardmann, R. F. P., and J. E. Booth, 1991, The significance of normal faults in the exploration and production of North Sea hydrocarbons, *in* A. M. Roberts, G. Yielding, and D. Freeman, The geometry of normal faults: Geological Society Special Publication, no. 56, p. 1–13.

Hubbert, M. K., 1953, Entrapment of petroleum under hydrodynamic conditions: AAPG Bulletin, v. 37, p. 1954–2026.

Jamison, W. R., and D. W. Stearns, 1982, Tectonic deformation of Wingate Sandstone, Colorado National Monument: AAPG Bulletin, v. 66, p. 2584–2608.

Kastning, E. H., 1977, Faults as positive and negative influences on ground-water flow and conduit enlargement, *in* R. R. Dilamarter and S. C. Csallany, eds., Hydrologic problems in karst regions: Bowling Green, Kentucky, West Kentucky University, p. 193–201.

Knipe, R. J., S. M. Agar, and D. J. Prior, 1991, The microstructural evolution of fluid flow paths in semi-lithified sediments from subduction complexes: Philosophical Transactions of the Royal Society of London A, v. 335, p. 261–273.

Logan, J. M., 1991, The influence of fault zones on crustal-scale fluid transport (abs.): AAPG Bulletin, v. 75, p. 623.

Maclay, R. W., and T. A. Small, 1983, Hydrostratigraphic subdivisions and fault barriers of the Edwards aquifer, south-central Texas, USA: Journal of Hydrology, v. 61, p. 127–146.

Malvern, L. E., 1969, Introduction to the mechanics of a continuous medium: Englewood Cliffs, New Jersey, Prentice-Hall, 713 p.

McCaig, A. M., 1989, Fluid flow through fault zones: Nature, v. 340, p. 600.

Montoto, L., 1982, Digital multi-image analysis: application to the quantification of rock microfractography: IBM Journal of Research and Development, v. 26, p. 735–745.

Moore, J. C., K. M. Brown, F. Horath, G. Cochrane, M. MacKay, and G. Moore, 1991, Plumbing accretionary prisms: effects of permeability variations: Philosophical Transactions of the Royal Society of London A, v. 335, p. 275–288.

Morrow, C. A., L. Q. Shi, and J. D. Byerlee, 1984, Permeability of fault gouge under confining pressure and shear stress: Journal of Geophysical Research, v. 89, p. 3193–3200.

Nelson, R. A., 1985, Geologic analysis of naturally fractured reservoirs: Houston, Texas, Gulf Publishing, 320 p.

Pittman, E. D., 1981, Effect of fault-related granulation on porosity and permeability of quartz sandstones, Simpson Group (Ordovician), Oklahoma: AAPG Bulletin, v. 65, p. 2381–2387.

Pittman, E. D., 1992, Relationship of porosity and permeability to various parameters derived from mercury injection-capillary pressure curves for sandstone: AAPG Bulletin, v. 76, p. 191–198.

Purcell, W. R., 1949, Capillary pressures—their measurements using mercury and the calculation of permeability therefrom: AIME Petroleum Transactions, v. 186, p. 39–48.

Quinn, B., 1988, Introducing Fast Montoto Thinning: Stanford Borehole Project, 162 p.

Rice, J. R., 1992, Fault stress states, pore pressure distributions, and the weakness of the San Andreas fault, *in* B. Evans and T.-F. Wong, eds., Fault mechanics and transport properties of rocks: San Diego, Academic Press, p. 475–503.

Schowalter, T. T., 1979, Mechanics of secondary hydrocarbon migration and entrapment: AAPG Bulletin, v. 63, p. 723–760.

Secor, D. T., 1965, Role of fluid pressure in jointing: American Journal of Science, v. 263, p. 633–646.

Seeburger, D. A., 1981, Studies of natural fractures, fault zones permeability and a pore space permeability model: Ph.D. thesis, Stanford University, Stanford, California, 243 p.

Seeburger, D. A., A. Aydin, and J. L. Warner, 1991, Structure of fault zones in sandstone and its effect on permeability (abs): AAPG Bulletin, v. 75, p. 669.

Shi, L. Q., C. Morrow, D. E. Moore, J. D. Bosrlee, 1980, Permeability of fault gouges under confining pressure and shear stress: EOS, v. 61, p. 1120.

Sleep, N. H., and M. L. Blanpied, 1992, Creep compaction and the weak rheology of major faults: Nature, v. 359, p. 687–692.

Smith, D. A., 1966, Theoretical considerations of sealing and nonsealing faults: AAPG Bulletin, v. 50, p. 363–374.

Smith, D. A., 1980, Sealing and nonsealing faults in Louisiana Gulf Coast Salt Basin: AAPG Bulletin, v. 64, p. 145–172.

Teufel, L. W., 1987, Permeability changes during shear deformation of fractured rock, *in* I. W. Farman, J. Daemen, C. S. Desai, C. E. Glass, and S. P. Neuman, Rock mechanics: Proceedings of the 28th U. S. Symposium on Rock Mechanics, v. 28, p. 473–480.

Watts, N. L., 1987, Theoretical aspects of cap-rock and fault seals for single- and two-phase hydrocarbon columns: Marine and Petroleum Geology, v. 4, p. 274–307.

Weber, K. J., and E. Daukoru, 1975, Petroleum geology of the Niger delta: Ninth World Petroleum Congress Transactions, v. 2, p. 209–221.

Zhao, G., and A. M. Johnson, 1991, Sequential and incremental formation of conjugate faults: Journal of Structural Geology, v. 13, p. 887–896.

Zieglar, D. L., 1992, Hydrocarbon columns, buoyancy pressures, and seal efficiency: comparisons of oil and gas accumulations in California and the Rocky Mountain area: AAPG Bulletin, v. 76, p. 501–508.

ABOUT THE AUTHORS

Marco Antonellini

Marco Antonellini has a degree in geological sciences from the University of Bologna (Italy). He worked for AGIP (1985–1988) in Italy and Egypt as a subsurface and structural geologist. After receiving an M.S. (1990) in geology from Michigan State University, he entered Stanford University where he is currently a Ph.D. candidate (geomechanics and structural geology). His research interests include reservoir characterization, fault geometry, and micromechanics of rock deformation.

Atilla Aydin

Atilla Aydin received his B.S. degree in geological engineering from Istanbul Technical University and his M.S. degree and Ph.D. in geology from Stanford University. His research interests include basin formation associated with strike-slip faults, faulting and jointing of rocks, permeability of faults, and characterization of fractured reservoirs. He has taught structural geology at Istanbul Technical University and Purdue University for 14 years. Presently, he is an associate professor (research) at Stanford University. He teaches a course in rock fracture and fracture flow and is the codirector of the Rock Fracture Project, an industrial affiliates program at Stanford.